Electromechanical characterization of carbon nanotubes in torsion via symmetry adapted tight-binding objective molecular dynamics

D.-B. Zhang,[1] R. D. James,[2] and T. Dumitrică[3,*]
[1]*Department of Chemical Engineering and Materials Science*
[2]*Department of Aerospace Engineering and Mechanics*
[3]*Department of Mechanical Engineering, University of Minnesota, Minneapolis, Minnesota 55455, USA*
(Received 15 June 2009; published 17 September 2009)

The nonlinear elastic response of carbon nanotubes (CNTs) in torsion is derived with objective molecular dynamics and a density-functional-based tight-binding model. The critical strain beyond which CNTs behave nonlinearly, the most favorable rippling morphology, and the twist- and morphology-related changes in fundamental band gap are identified from a rigorous atomistic description. There is a sharply contrasting behavior in the electronic response: while in single-walled CNTs the band-gap variations are dominated by rippling, multiwalled CNTs with small cores exhibit an unexpected insensitivity. Results are assistive for experiments performed on CNT-pedal devices.

DOI: 10.1103/PhysRevB.80.115418 PACS number(s): 73.63.Fg, 61.48.De, 71.15.Pd, 85.85.+j

I. INTRODUCTION

Carbon nanotubes (CNTs) are attractive components in nanoelectromechanical devices[1] and the change in their electronic properties under mechanical deformations has been under intense scrutiny.[2–7] It is now possible to perform conductivity measurements in CNT-pedal devices which employ CNTs as torsional springs.[8–13] Since experimental uncertainties are numerous, a theoretical understanding of the response of an individual CNT can help interpret the experimental data. Here we report quantum-mechanical (QM) atomistic calculations that reveal important electromechnical differences between the torsional behavior of single-walled (SW) and multiwalled (MW) CNTs. Close to their operating points in nanodevices, CNTs develop rippling deformations.[14,15] The idealized model of Yang and Han,[16] which assumes a homogeneous torsional strain, is widely used to rationalize the intrawall band-gap variations with twist.[11–13] Assessing the validity of this model under rippling is another outcome of this research.

Rippling is a complex elastic deformation. It represents a way of lowering energy by creating an inhomogeneous torsional strain coupled with the development of helicoidal ridges and furrows of positive and negative curvatures, respectively. Due to the distributed nature, the long-range interwall interactions are also perturbed. For high fidelity modeling, accurate accounting of both covalent and van der Waals forces is needed. In principle, QM calculations can provide both the morphological changes and the electronic behavior. There is ample evidence that an explicit QM treatment of bonding gives an accurate description of CNT's mechanics.[17–20] However, the usual translation-invariant formulation is computationally prohibitive for long-range elastic deformations with helical symmetry. To reduce the computational complexity, empirical classical potentials[21–24] and continuum idealizations derived from classical potentials[14,15,25] are widely used. When compared with QM descriptions, these approaches are sometimes inaccurate, including for describing the linear elastic regime.[18,19] Another obvious disadvantage is that the electronic response is not revealed.

II. METHODOLOGY

To make accessible QM studies accessible we used objective molecular dynamics (MD), a versatile methodology applied before in linear elasticity[18] and plasticity[26] studies of CNTs exposed to torsion. Below, we give the necessary simulation details and highlight the distinct ingredients of our method. A rigorous justification is given in Ref. 27.

In standard MD under periodic boundary conditions (PBC), the dynamic solution satisfies the specified translational invariance of an infinitely long CNT. As a result, only atoms located in one PBC cell are subjected to Newton's equations of motion, and atoms from all other cells adopt positions according to the assigned periodicity. In the objective MD generalization, helical symmetry is instead considered and only the N_0 atoms located at positions $\mathbf{X}_j$ in the initial objective cell are followed. Since the objective MD solution is invariant to an assigned set of helical and angular operations, atoms $\mathbf{X}_{j,\zeta_1,\zeta_2}$ located in the objective cell indexed by integers ζ_1 and ζ_2, adopt the positions given by[27,28]

$$\mathbf{X}_{j,\zeta_1,\zeta_2} = \mathbf{R}_2^{\zeta_2}\mathbf{R}_1^{\zeta_1}\mathbf{X}_j + \zeta_1\mathbf{T}_1, \quad j = 1, \ldots, N_0. \tag{1}$$

Rotational matrix $\mathbf{R}_1$ of angle θ_1 combined with axial vector $\mathbf{T}_1$ characterize the helical transformation while matrix $\mathbf{R}_2$ indicates an angular rotation with angle θ_2. It is most interesting to examine the strain-electronic energy relationship in armchair CNTs as they undergo metal-to-semiconductor transition under mechanical deformation.[5,6,13] Thus, we are concerned only with armchair CNTs for which $\mathbf{T}_1 = \mathbf{T}$ and $\theta_1 = 0$. We set $\theta_1 = \gamma|\mathbf{T}|$ to impose a torsional strain rate γ. Depending on the selected objective cell, θ_2 is $360°/n$ or a multiple of it.

In our symmetry-adapted tight-binding of objective MD, the interatomic interactions are accounted for with the extended density-functional theory-based nonorthogonal two-center parameterization of carbon.[19,29,30] This tight-binding model describes well the electromechanical[17–19,31] response of CNTs, including in laterally squeezed CNTs.[6]

Let N_s be the number of helical operations (typically ∞) over which the cyclic boundary conditions are imposed and

N_a the finite number of θ_2 rotations that fill the CNT circumference. The electronic states are represented by linear combinations of symmetry-adapted Bloch sums[28]

$$|\alpha j, l\kappa\rangle = \frac{1}{\sqrt{N_a \cdot N_s}} \sum_{\zeta_1=0}^{N_s-1} \sum_{\zeta_2=0}^{N_a-1} e^{il\theta_2\zeta_2 + i\kappa\zeta_1} |\alpha j, \zeta_1\zeta_2\rangle. \quad (2)$$

The Bloch factors are eigenvalues of the commuting rotation and helical operators. Index $l=0,1,\ldots,N_a-1$ is the angular quantum number, labeling the standing electronic waves in the circumferential direction, and $-\pi \leq \kappa < \pi$ is the helical wavevector already normalized by the helical periodicity. $|\alpha j, \zeta_1\zeta_2\rangle$ is the orbital with symmetry α located on atom j, all in the objective cell indexed by ζ_1 and ζ_2. The force on each atom j is computed from the electronic-band energy using the Hellmann-Feynman theorem.[28]

To identify the optimal rippling configurations, objective MD was used as an optimization tool by carrying out a combination of room-temperature MD with a 1 fs time step, followed by conjugate-gradient energy minimizations. Between 5 (for MD) and 100 (for structural relaxations) κ points and all l points were used to converge the band energy.

III. SIMULATION RESULTS

A. Single-walled CNTs

We begin by discussing SWCNTs in torsion under the constraint of constant length. Renouncing the translational symmetry allowed us to compute in an economical fashion the expected helical[14,15,25] rippling morphologies that characterize the initial stages[25] of the nonlinear elastic response. For example, the wavelike modes for (12,12) SWCNT shown in Fig. 1(a), were individually computed with objective MD from three objective cells delineated by the translational vector **T** but different θ_2 values, 180°, 120°, and 90°. Because these cells contain only 24, 18, and 12 atoms, respectively, the tight-binding treatment can be comfortably applied.

Relying on the symmetry constraints, we studied in a decoupled way the various rippling morphologies, unambiguously identified the fundamental (lowest-energy) mode, and pinpointed the level of twist beyond which the cylinder shape becomes first unstable, i.e., the bifurcation point. The importance range of the various modes can be determined from Fig. 1(b), which shows the computed strain-energies vs γ. The curve obtained from a 4 atom objective cell with $\theta_2 = 30°$ (thin line) is a useful reference as the SWCNT's cylinder shape is preserved. At lower strains this state is stable but when strain exceeds 4°/nm the two-lobe rippling significantly lowers the elastic energy. The perfect structure can also assume the three- and four-lobe buckled states beyond 7°/nm and 9°/nm, respectively, but the two-lobe morphology stays favorable by a large margin. We conjecture that the various wavelike modes shown in Fig. 1(a) exist as distinct metastable states and twisting doesn't mix them.

The evolution of torque (energy derivative with γ), Fig. 1(b), further reveals that the two-lobe rippling develops in two stages. The first is a *transient* one and initiates at the bifurcation, where the linear torque variation is interrupted

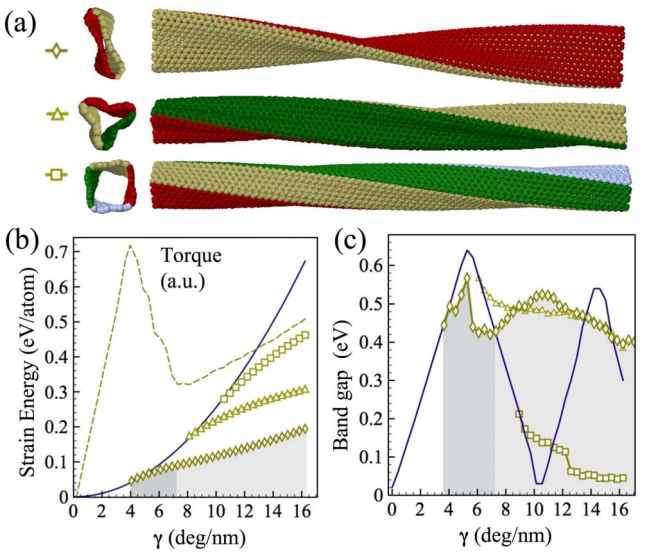

FIG. 1. (Color online) (a) Rippling patterns in a (12,12) SWCNT under 10°/nm twist. Colors correspond to azimuthal replicas of the objective cell. (b) Strain energy and (c) band gap vs twist rate γ for cylinder idealized shape and rippling modes. Torque (in arbitrary units) for the two-lobe mode reveals two stages of rippling, marked with two gray levels.

by a rather abrupt drop. The cylinder shape develops ridges and furrows as the torque's rate of change is negative. The minimum distance between furrows decreases until the van der Waals equilibrium distance of 3.4 Å is reached at 7.2°/nm. Here the transient stage is completed and torque's rate of growth switches from negative to positive. In this second stage there is no notable change in shape of the collapsed cross section.

Figure 1(c) shows the variations in the electronic band gap for the idealized cylinder and rippling modes. Band-gap information is important because of the relationship with the experimentally relevant CNT resistance.[12] For the idealized case, the band gap is periodically modulated. During one period $\Delta\gamma$, it grows in a linear fashion, reaches a maximum at halfway, then decreases to zero. These features are in agreement with the predictions of Yang and Han[16] developed from the band structure of graphene: Uniformly twisted SWCNTs are metallic only when the metallic wave function of graphene is commensurated with the SWCNT's circumference. Otherwise they are semiconducting. Due to the linearity of the dispersion relation of graphene near its Fermi level, band gap varies in a linear fashion with a $3t_0R$ slope. R is the SWCNT's radius and t_0 is the tight-binding hopping element. It also follows[16] that $\Delta\gamma = d_{C\text{-}C}/R^2$, where $d_{C\text{-}C}$ is the C-C bond length. Fitting to our data gives $t_0 = 2.72$ eV and $d_{C\text{-}C} = 1.42$ Å, in agreement with the actual values of these parameters.

It is instructive to identify for the idealized case the twist-related changes in the electronic band structure, Fig. 2(a). In the stress-free case, the metallic character is due to the intersection of the nondegenerate $l=0$ valence and conduction bands. Note that most bands in the stress-free structure appear double degenerate due to symmetry. Twisting removes degeneracies, opens a fundamental direct gap between $l=0$

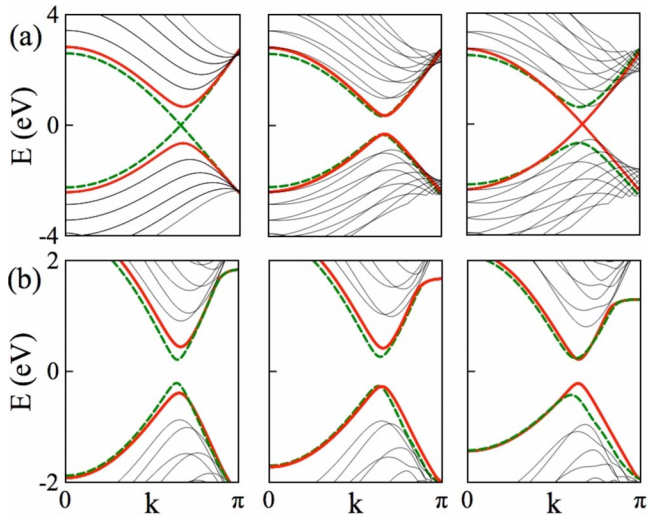

FIG. 2. (Color online) Electronic-band dispersion in (12,12) SWCNT, for two shapes and several γ values: (a) cylinder idealized stress-free (left), 5 deg/nm (middle), and 10.5 deg/nm (right), and (b) two-lobe rippling 6 deg/nm (left), 10.5 deg/nm (middle), and 16 deg/nm (right). Thick dashed (green) and continuous (red) bands have l of 0 and 1, respectively.

valence and conduction and decreases the gap between $l=1$ valence and conduction. Beyond 5.5 deg/nm, the gap is still direct and given by the $l=1$ bands. The metallic character is regained when $l=1$ bands intersect.

When accounting for rippling the band gap for all modes undergoes major changes, which are distinct from the idealized predictions. Focusing on the two-lobe mode in Fig. 1(c), we note that in the transient mechanical stage (dark gray shaded) band gap departs only slightly from the idealized model. Immediately after bifurcation, when the formation of ridges is initiated, the band gap exhibits a small decrease. The sudden onset of inhomogeneous strain manifested in the creation of furrows is reflected in a ~0.15 eV band-gap drop. Note that in this process the minimum distance between furrows drops from 10.3 Å to 6 Å, not enough to cause electronic coupling. Next, as rippling becomes pronounced and the distance between furrows decreases rapidly, reaching ~3.4 Å at 7.2°/nm, the band gap maintains a constant value. This indicates that the now present electronic coupling between faces and the inhomogeneous strain effect cancel each other.

In the second mechanical stage of rippling (light gray shaded), the idealized model of the band-gap variations is not applicable. The noted slow band-gap increase when strain exceeds 7.2°/nm is still twist related, as can be seen from the evolution of the band structure shown in Fig. 2(b). Due to the perturbation caused by the formation of ridges the characteristic switching of bands occurs sequentially: under 11°/nm at the maximum band gap of 0.54 eV there is a switching of $l=0$ and 1 valence bands, followed by a slow band-gap decrease. The gap stays indirect until the switching of $l=0$ and 1 conduction bands at 16°/nm.

The generality of the above behavior is demonstrated in Fig. 3, which summarizes results from a series of similar calculations performed on armchair CNTs. During torsion

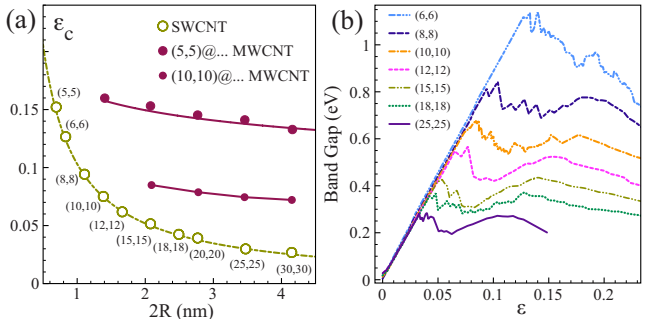

FIG. 3. (Color online) (a) Critical shear strain vs CNT's diameter for SW (open circles) and MW (full circles) armchair CNTs. (b) Changes in the band gap with the shear strain for armchair SWCNTs.

the ideal SWCNT wall experiences a shear strain $\varepsilon=\gamma R$. Figure 3(a) plots the obtained critical shear for rippling ε_c, which exhibits a scaling $\varepsilon_c=0.1([\text{nm}]/2R)^{0.99}$ qualitatively inconsistent with the $\sim R^{-3/2}$ dependence[24] obtained from atomistic simulations using classical potentials and different boundary conditions. Figure 3(b) reveals the band-gap dependence with ε. In agreement with the idealized model, the linear regime data collapses onto a common line with a $3t_0$ slope. However, beyond ε_c, the idealized model based on the homogeneous strain assumption cannot be used. Data suggests that small-amplitude large-period band-gap oscillations can still occur due to the switching of the $l=0$ and 1 bands exhibited by the two-lobe mode.

B. Multiwalled CNTs

The computed band-gap changes correlate well with the linear variations in conductivity measured in torsionally deformed SWCNTs[12] under $\varepsilon<0.025$. Similar measurements in MWCNTs obtained conductance oscillations[11] that were attributed to the idealized metal-semiconductor oscillations occurring in the outer wall.[13] In SWCNTs metal-semiconductor oscillations cannot occur before bifurcation since $\Delta\gamma>\varepsilon_c/R$ and the idealized model cannot be used for the rippling state. Thus the experimental evidence combined with our SWCNT data suggests that MWCNTs must have a different electromechanical behavior.

To investigate this hypothesis we carried out objective MD calculations on two MWCNT families (5,5)@(10,10)@…@(5n,5n) and (10,10)@…@(5n,5n), with $n\in\{3,\ldots,6\}$, all represented by their PBC unit cells. We obtained that the nonlinear regime is still governed by a two-lobe mode, as exemplified in Fig. 4, for the (5,5)@(10,10)@(15,15) MWCNT. Modes with larger angular wave numbers such as the previously identified five-lobe mode[15] shown in Fig. 4(a), were retrieved at larger γ values but were less favorable energetically.

Like in SWCNTs, the development of the two-lobe rippling mode involves a transient stage. As expected from the scaling obtained for SWCNTs, rippling in MWCNTs initiates in the outermost wall. This leads to a first discontinuity in torque, Fig. 4(a). Interestingly, the bifurcation value of 8.1 deg/nm is significantly larger than the 2.8 deg/nm critical

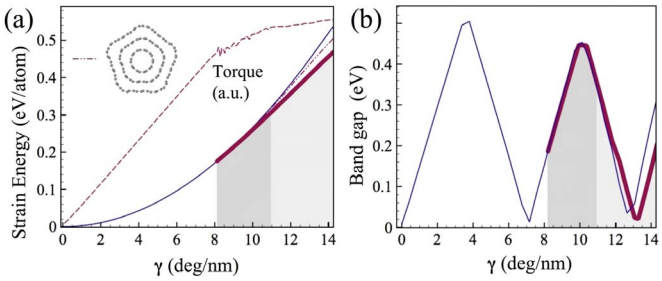

FIG. 4. (Color online) Rippling in a (5,5)@(10,10)@(15,15) MWCNT (a) Strain energy and (b) band gap (outer wall) vs twist rate for the cylinder idealized shape (thin line) and two-lobe (thick line) and five-lobe (dash-dot-dot line) rippling modes. Torque (dashed line) for the two-lobe mode reveals two stages of rippling, marked with two gray levels.

strain of isolated (15,15) SWCNT. Next, rippling propagates toward the core. By the time the transient regime is completed at 10.9 deg/nm all walls exhibit some degree of rippling, as can be seen from the cross-sectional view presented in Fig. 5(a). The following linear increase in torque reflects the second rippling stage identified previously by coarse-grained simulations.[15]

Unlike in SWCNTs, the band gap shown in Fig. 4(b) follows closely the band-gap variations of the idealized outer wall. There is one metal-semiconductor oscillation before bifurcation and the oscillatory behavior continues even after the transient stage of rippling. Similar metal-semiconductor oscillations (not shown) have been observed for rippling morphologies with higher angular numbers.

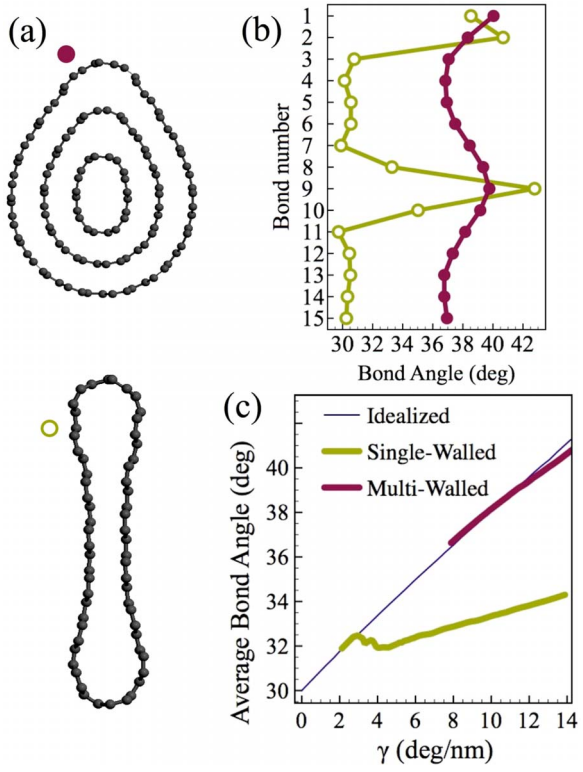

FIG. 5. (Color online) (a) Rippling in (5,5)@(10,10)@(15,15) MWCNT under 11 deg/nm. Analysis of the outermost wall: (b) circumferential distribution of the angle made by family of C-C bonds initially tilted at 30° with respect to the long axis. Strain is 11 deg/nm. (c) Evolution of the average angle for the same C-C bonds with the applied torsion. The (15,15) SWCNT cases (ideal and rippling) are shown for comparison.

C. Discussion

To summarize, objective MD simulations revealed an intriguing electromechanical aspect. Although mechanically SWCNTs and MWCNTs exhibit a qualitatively similar nonlinear elastic behavior, their electronic response is markedly different. This difference can be rationalized as follows.

In comparison with the isolated SWCNT case, the presence of inner walls in MWCNTs modifies the response of the outer wall in two important ways:

(i) The strain at the bifurcation is overall appreciably higher than the one for the isolated outer wall, Fig. 3(a). The size effect is subtle and the bifurcation strain is largely set by the size of the wall at the core. Note that the scaling $\varepsilon_c = 0.16([\text{nm}]/2R)^{0.15}$ obtained for the MWCNT family containing the (5,5) core is different from the coarse-grained $\sim 1/R$ scaling derived recently for thick MWCNTs.[15] Band gap oscillations are possible before bifurcation as $\Delta\gamma < \varepsilon_c/R$ for $R > 1$ nm.

(ii) Rippling is significantly faded, Fig. 5. To obtain insight into the homogeneity of the torsional strain of the outer wall we examined the angle made by family of C-C bonds that were initially tilted at 30° with respect to the CNT axis. Figure 5(b) compares the rippling morphology of the outermost wall in (5,5)@(10,10)@(15,15) MWCNT with the one encountered in the isolated (15,15) SWCNT at the same level of strain. While there is a highly inhomogeneous strain distribution in the collapsed (15,15) SWCNT, strain appears largely homogenous when the two inner layers were present. Figure 5(c) indicates that throughout deformation the torsional strain in the outermost wall closely resembles the idealized behavior.

IV. SUMMARY

In spite of the experimental interest, modeling CNTs in torsion has been challenging and most of our understanding comes from classical potential and continuum mechanics approaches. Here we showed that to obtain QM insight, it is not essential to enlarge the size range (in terms of number of atoms) covered currently with QM methods. Giving up on the standard translational symmetry is the key to directly account for the interplay between the classical ionic and QM electronic degrees of freedom in a CNT under an arbitrary twist and without introducing unwanted end effects.

Using objective MD coupled with extended density-functional theory-based nonorthogonal tight binding we characterized in significant detail the linear and nonlinear elastic response of a large collection of infinitely long armchair CNTs up to 5 nm in diameter. We uncovered a sharply contrasting electromechanical behavior. On one hand, SWCNTs are prone to significant rippling with the smaller diameter tubes being more stable than larger ones. Rippling

is reflected immediately in the electronic states. The experimentally relevant twist-induced band-gap variations can no longer be described by the widely used idealized model,[16] which assumes homogeneous torsional strain. Thus, from an electromechanical perspective SWCNTs are less suitable for their perfect cylinder idealization. On the other hand, MWCNTs behave as a set of coaxial cylinders over a large torsional strain range. Although rippling initiates in the outer wall, the bifurcation strain is largely set by the size of the tube at the core. As a result, the outer wall preserves its cylinder shape longer especially in thick MWCNTs with small cores. Even beyond bifurcation due to the support provided by the inner walls rippling is inhibited to the extent that its influence on the band gap is only perturbative. The band gap in the outer wall varies like in an isolated cylindrical tubule of same diameter. Contrary to expectations, the formalism of Yang and Han[16] initially developed for isolated SWCNTs turns out to be more applicable for MWCNTs.

ACKNOWLEDGMENTS

D.-B.Z. and T.D. thank NSF CAREER under Grant No. CMMI-0747684, AFOSR Grant No. FA9550-09-1-0339, and the Donors of the American Chemical Society Petroleum Research Fund. R.D.J. acknowledges support from AFOSR (GameChanger, Grant No. GRT00008581/RF60012388, and Grant No. FA9550-09-1-0339), NSF (Grant No. DMS-0757355), and DOE (Grant No. DE-FG02-05ER25706). Computations were carried out at the Minnesota Supercomputing Institute.

*Corresponding author; td@me.umn.edu

[1] V. Sazonova, Y. Yaish, H. Ustunel, D. Roundy, T. A. Arias, and P. L. McEuen, Nature (London) **431**, 284 (2004).
[2] T. W. Tombler, C. W. Zhou, L. Alexseyev, J. Kong, H. J. Dai, L. Lei, C. S. Jayanthi, M. J. Tang, and S. Y. Wu, Nature (London) **405**, 769 (2000).
[3] E. D. Minot, Y. Yaish, V. Sazonova, J.-Y. Park, M. Brink, and P. L. McEuen, Phys. Rev. Lett. **90**, 156401 (2003).
[4] C. Gomez-Navarro, J. J. Saenz, and J. Gomez-Herrero, Phys. Rev. Lett. **96**, 076803 (2006).
[5] P. E. Lammert, P. Zhang, and V. H. Crespi, Phys. Rev. Lett. **84**, 2453 (2000).
[6] H. Mehrez, A. Svizhenko, M. P. Anantram, M. Elstner, and T. Frauenheim, Phys. Rev. B **71**, 155421 (2005).
[7] J.-Q. Lu, J. Wu, W. Duan, F. Liu, B.-F. Zhu, and B.-L. Gu, Phys. Rev. Lett. **90**, 156601 (2003).
[8] A. M. Fennimore, T. D. Yuzvinsky, W.-Q. Han, M. S. Fuhrer, J. Cumings, and A. Zettl, Nature (London) **424**, 408 (2003).
[9] J. C. Meyer, M. Paillet, and S. Roth, Science **309**, 1539 (2005).
[10] A. R. Hall, L. An, J. Liu, L. Vicci, M. R. Falvo, R. Superfine, and S. Washburn, Phys. Rev. Lett. **96**, 256102 (2006).
[11] T. Cohen-Karni, L. Segev, O. Srur-Lavi, S. R. Cohen, and E. Joselevich, Nat. Nanotechnol. **1**, 36 (2006).
[12] A. R. Hall, M. R. Falvo, R. Superfine, and S. Washburn, Nat. Nanotechnol. **2**, 413 (2007).
[13] K. S. Nagapriya, S. Berber, T. Cohen-Karni, L. Segev, O. Srur-Lavi, D. Tománek, and E. Joselevich, Phys. Rev. B **78**, 165417 (2008).
[14] M. Arroyo and T. Belytschko, Phys. Rev. Lett. **91**, 215505 (2003).
[15] I. Arias and M. Arroyo, Phys. Rev. Lett. **100**, 085503 (2008).
[16] L. Yang and J. Han, Phys. Rev. Lett. **85**, 154 (2000).
[17] E. Hernandez, C. Goze, P. Bernier, and A. Rubio, Phys. Rev. Lett. **80**, 4502 (1998).
[18] D.-B. Zhang and T. Dumitrică, Appl. Phys. Lett. **93**, 031919 (2008).
[19] A. Carlson and T. Dumitrică, Nanotechnology **18**, 065706 (2007).
[20] T. Dumitrică, M. Hua, and B. I. Yakobson, Proc. Natl. Acad. Sci. U.S.A. **103**, 6105 (2006).
[21] B.-W. Jeong, J.-K. Lim, and S. B. Sinnott, J. Appl. Phys. **101**, 084309 (2007).
[22] Q. Wang, Nano Lett. **9**, 245 (2009).
[23] A. Rochefort, P. Avouris, F. Lesage, and D. R. Salahub, Phys. Rev. B **60**, 13824 (1999).
[24] T. Chang, Appl. Phys. Lett. **90**, 201910 (2007).
[25] B. I. Yakobson, C. J. Brabec, and J. Bernholc, Phys. Rev. Lett. **76**, 2511 (1996).
[26] D.-B. Zhang, R. D. James, and T. Dumitrică, J. Chem. Phys. **130**, 071101 (2009).
[27] T. Dumitrică and R. D. James, J. Mech. Phys. Solids **55**, 2206 (2007).
[28] D.-B. Zhang, M. Hua, and T. Dumitrică, J. Chem. Phys. **128**, 084104 (2008).
[29] D. Porezag, Th. Frauenheim, Th. Köhler, G. Seifert, and R. Kaschner, Phys. Rev. B **51**, 12947 (1995).
[30] R. Rurali and E. Hernandez, Comput. Mater. Sci. **28**, 85 (2003).
[31] V. N. Popov and L. Henrard, Phys. Rev. B **70**, 115407 (2004).